ISSN 2070-0504, Catalysis in Industry, 2018, Vol. 10, No. 1, pp. 1–8. © Pleiades Publishing, Ltd., 2018.
Original Russian Text © G.I. Konstantinov, S.S. Kurdyumov, Yu.V. Maksimov, O.V. Bukhtenko, M.V. Tsodikov, 2018, published in Kataliz v Promyshlennosti.

CATALYSIS IN CHEMICAL AND PETROCHEMICAL INDUSTRY

Hydrogen Sulfide-Resistant Bifunctional Catalysts for the Steam Reforming of Methane: Activity and Structural Evolution

G. I. Konstantinov[a], *, S. S. Kurdyumov[a], **, Yu. V. Maksimov[b], *, O. V. Bukhtenko[a], ****, and M. V. Tsodikov[a], *******

[a] *Topchiev Institute of Petrochemical Synthesis, Russian Academy of Sciences, Moscow, 119991 Russia*
[b] *Semenov Institute of Chemical Physics, Russian Academy of Sciences, Moscow, 117977 Russia*
**e-mail: konstantinov@ips.ac.ru*
***e-mail: kurdyumov@ips.ac.ru*
****e-mail: maksimov@chph.ras.ru*
*****e-mail: bukhtenko@ips.ac.ru*
******e-mail: tsodikov@ips.ac.ru*

Received March 28, 2017

Abstract—Results are presented from studying an iron–nickel catalyst for the steam reforming of methane, synthesized by epitaxial coating on the surface of spherical pellets of commercial γ-Al_2O_3. It is shown the catalyst is resistant to the presence of hydrogen sulfide in a steam–gas mixture. The degree of conversion of methane during reforming is close to equilibrium at a pressure of 2.0 MPa, a temperature of 800°C, a ratio of $H_2O : CH_4 = 2 : 1$, a feedstock hourly space velocity (FHSV) of 6000 h^{-1}, and a H_2S concentration of 30 ppm. The structural evolution and phase state of the active components of the system are studied via X-ray diffraction analysis, transmission electron microscopy (TEM), and Mössbauer spectroscopy. The formation of paramagnetic iron oxide clusters tightly bound to the structure of the support, and of $FeNi_3$ iron–nickel alloy particles on the surface of the catalyst, is responsible for the polyfunctional properties of the catalyst, which displays high activity in both the steam reforming of methane and the oxidative decomposition of hydrogen sulfide to elemental sulfur.

Keywords: steam reforming, methane, hydrogen sulfide, hydrogen, core–shell, nickel
DOI: 10.1134/S2070050418010063

INTRODUCTION

The steam reforming of hydrocarbon feedstocks is the most cost-effective and thus most commonly used means of all those currently available for the production of hydrogen and synthesis gas.

The stringent conditions of the steam reforming process impose a number of requirements on both the catalysts and the catalyst supports. An insufficient amount of steam supplied during methane reforming thus intensifies coking, which first deactivates the catalyst and then degrades the catalyst pellets.

Another important requirement imposed on catalysts for the steam reforming of natural hydrocarbon feedstocks and fuel hydrocarbons is resistance to sulfur-containing compounds. With most commercial catalysts for the steam reforming of natural hydrocarbon feedstocks, poisoning with sulfur-containing compounds causes a rapid loss of activity. Resistance to sulfur poisoning is one of the most important characteristics of catalyst systems used in the steam reforming of hydrocarbons. It is known that even after the preliminary hydrotreating stage, the feedstock contains a certain amount of sulfur that can adversely affect the activity of catalyst systems.

The most thoroughly studied and commonly used catalysts for the steam reforming of methane (SRM) are nickel systems. In addition to nickel, other metals of group VIII can catalyze the SRM process: Rh, Ru, Ir, Pt, Pd, Co, and Fe [1–6]. However, iron and cobalt are subject to oxidation and deactivation under conditions of SRM. Catalysts based on platinum group metals are less prone to deactivation due to carbon deposition and the presence of sulfur compounds in the converted feedstock. However, analysis of the data on the steam reforming of hydrocarbons in the presence of these catalysts shows that nickel catalyst samples deposited on different supports that are typically made of Al_2O_3, MgO, ZrO, and TiO_2 oxides are more effective and more commonly used in industry because of their low cost (100–150 times less expensive) [7].

Table 1. Composition of the supports prepared via impregnation

Sample number	Component content, wt %			
	Al_2O_3	Fe_2O_3	MgO	substrate
1	13.35	6.75	12.59	67.31
2	14.15	9.44	7.86	68.55
3	11.82	7.88	6.57	73.73
4	11.85	5.98	11.17	71.00
5	13.01	6.57	12.58	67.84
6	13.63	6.89	12.13	67.35

According to the authors of [8–10], the presence of La compounds in the structure of an SRM catalyst improves the catalyst's resistance to coking. This is attributed to the formation of lanthanum oxocarbonate and the subsequent reaction of this compound with the formed carbon according to the equation

$$La_2O_2CO_3 + C_{surf} = 2CO + La_2O_3.$$

According to the authors of [10], another factor that increases a catalyst's activity in the reforming process is an increase in the degree of dispersion of Ni particles upon the introduction of lanthanum.

Results from studying catalyst systems based on vermiculite ore in the SRM process were presented in [8, 11]. It was found that after heat treatment, a support prepared via precipitation from vermiculite ore acidic etching solutions has the well-crystallized structure of $Mg(FeAl)O_{4\pm\delta}$ spinel and is a promising support for catalysts used in the steam reforming of hydrocarbon feedstocks. Studies of the evolution of catalyst structure show that after the deposition of Ni–La active components and reductive activation with hydrogen, hybrid nanoparticles with core–shell configurations form on a catalyst's surface. The core is composed of Fe–Ni alloy particles of 12–15 nm in size and is surrounded by a shell composed of superparamagnetic γ-Fe_2O_3 clusters of 1–4 nm in size.

To improve catalysts and increase their mechanical strength and thermal stability, we studied the mechanism of the formation of a new model catalyst system based on γ-Al_2O_3 with the same composition of the active components of the surface as that of a sample based on vermiculite ore and developed approaches to synthesizing the catalyst. This catalyst can be used either in a fixed bed or in moving and fluidized beds, making it much easier to solve problems of heat and mass transfer.

It should also be noted that the composition of vermiculite feedstock can vary, depending on the location of the ore vein. It is therefore important to search for synthesis approaches to designing active components based on purified reagents for preparing catalysts with desired chemical and phase compositions [12].

In this work, we present the results from studying the activity and resistance to sulfur of an iron–nickel SRM catalyst prepared with epitaxial coating on the surfaces of commercial spherical γ-Al_2O_3.

EXPERIMENTAL

Preparing a γ-Al_2O_3-Based Catalyst Support

Our support was prepared by impregnating spherical γ-Al_2O_3 pellets of 3.0–3.2 mm in size (AO SKTB Katalizator, Novosibirsk) that served as the substrate. The water uptake of the substrate was determined before deposition (1.02 cm^3/g).

The precursors used to prepare aqueous solutions for impregnating the substrate were aluminum, iron, and magnesium nitrates purchased from Sigma-Aldrich and dissolved in distilled water: $Al(NO_3)_3 \cdot 9H_2O$ (high-purity grade), $Fe(NO_3)_3 \cdot 9H_2O$ (high-purity grade), and $Mg(NO_3)_2 \cdot 6H_2O$ (analytical grade). The Al_2O_3 : Fe_2O_3 : MgO weight ratio corresponded to the one in supports prepared from vermiculite ore etching solutions [8]. The total metal concentration in the solution was 36.5 g/L (samples 1, 4, 5, 6) and 42 g/L (samples 2, 3) due to an increase in the Fe^{3+} content.

The layer-by-layer deposition of an aqueous solution containing aluminum, iron, and magnesium nitrates was developed to increase the volume of the deposited metals. Each layer was deposited via wet impregnation, according to data on the water uptake of the substrate. After the deposition of each layer, the sample was held in a sealed container with continuous shaking for 2 h. The sample was next dried in a fume hood with a stream of warm air and then in a drying oven at a temperature of 120°C for 30 min. After this, it was subjected to a thermal shock by placing the sample in a muffle furnace heated to a temperature of 200°C. The temperature was adjusted to 500°C at a rate of 10°C/min and held at this level for 30 min. Finally, the sample was cooled in a desiccator, weighed, and coated with the next layer.

Ten layers were deposited using this procedure. After deposition of the last layer, the sample was air-dried at room temperature, then dried in a drying oven at 120°C for 5 h, and finally subjected to stepwise heat treatment at 500°C for 5 h, 600°C for 1 h, 800°C for 4 h, 850°C for 2 h, and 900°C for 1 h.

The composition of the synthesized catalysts was determined via atomic absorption spectrometry using a PerkinElmer AAnalyst 400 unit. The composition of the prepared supports is shown in Table 1.

Preparation of Nickel–Lanthanum Catalyst

Nickel–lanthanum catalysts were prepared via two-stage impregnation. The lanthanum source was lanthanum nitrate salt $La(NO_3)_3 \cdot 6H_2O$ (high-purity grade, Sigma-Aldrich); the nickel source was nickel

Table 2. Composition of the catalysts prepared via impregnation

Sample number	Active components, wt %		Support, wt %			Substrate, wt %
	NiO	La_2O_3	Al_2O_3	Fe_2O_3	MgO	γ-Al_2O_3
1	10.72	4.95	11.26	5.69	10.62	56.76
2	10.40	4.95	11.41	7.61	6.34	59.25
3	10.18	4.94	10.03	6.69	5.58	62.58
4	11.91	4.80	9.71	4.91	9.16	59.51
5	10.82	5.71	10.17	5.14	10.47	57.69
6	10.85	5.34	10.90	5.50	10.29	57.12

nitrate salt $Ni(NO_3)_2 \cdot 6H_2O$ (analytical grade, Sigma-Aldrich).

At the first stage, the support was impregnated with an aqueous solution of lanthanum nitrate in the concentration required to deposit ≈5 wt % of La_2O_3; the duration of exposure was 2 h. The impregnated pellets were next dried in air and then in a drying oven at 120°C for 6 h. Finally, they were subjected to calcination in a muffle furnace at 800°C for 2 h.

At the second stage, nickel was deposited via impregnation with an aqueous solution of nickel nitrate in a concentration of ≈11 wt % (in terms of NiO); the duration of exposure was 2 h. The impregnated pellets were next dried in the air and then in a drying oven at 120°C for 6 h. Finally, they were subjected to calcination in a muffle furnace at 500°C for 5 h.

The concentrations of the lanthanum nitrate and nickel nitrate solutions were calculated according to the predetermined water uptake of the supports and the required La_2O_3 and NiO content in the catalyst.

Table 2 presents the composition of the resulting catalysts.

Determining Catalyst Activity

The catalyst activity in the SRM process was determined in a flow system that allowed real-time analysis of the products. The SRM system is schematized in Fig. 1.

The catalyst in the amount of 12 cm^3 was charged into a heat-resistant steel reactor with a diameter of 30 mm. They were then subjected to reductive conditioning in a hydrogen stream at a temperature of

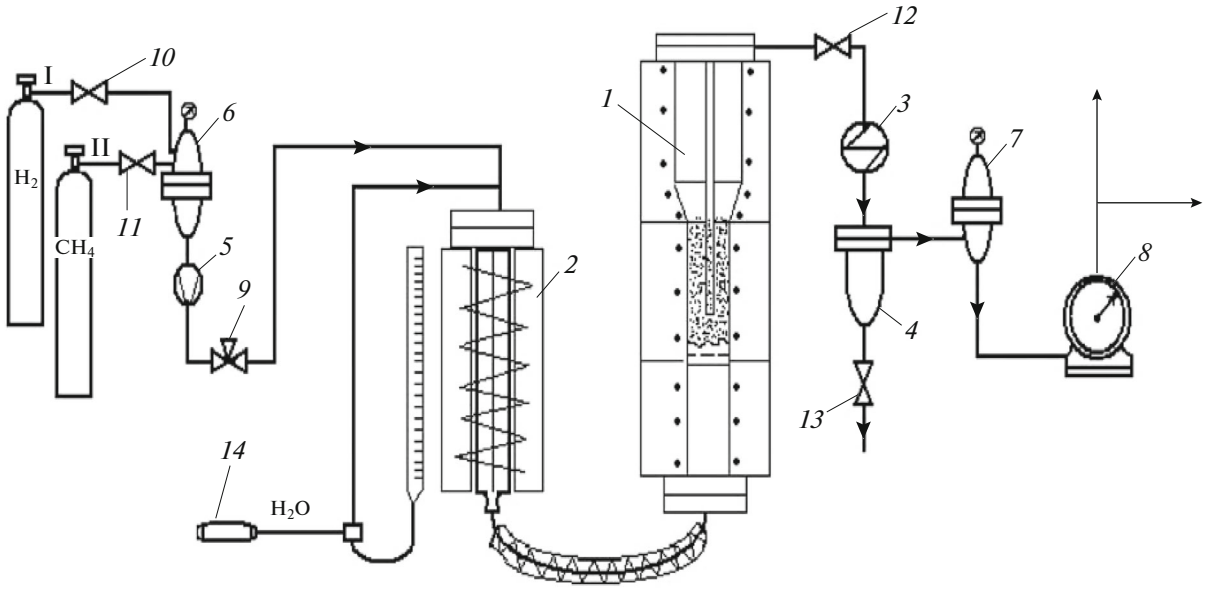

Fig. 1. Our system for determining the catalyst activity in the steam reforming of hydrocarbons: (*1*) reactor; (*2*) heating unit; (*3*) condensing and cooling unit; (*4*) separator; (*5*) flow rate meter; (*6*, *7*) pressure controller; (*8*) wet gas meter; (*9*) fine adjustment valve; (*10*–*13*) shut-off valves; (*14*) NZhR pump.

800°C for 3 h. Steam from a heating unit was next supplied to the reactor in addition to hydrogen. Upon reaching the operating temperature, the hydrogen supply was cut off, and pure methane or a steam–gas mixture of methane and hydrogen sulfide was fed into the reactor. Our tests were conducted at a pressure of 2.0 MPa; a temperature of 800°C; an $H_2O : CH_4$ ratio of 2 : 1; and FHSV of 6000 h^{-1}. Through an automatic four-port back-purging check valve, a portion of the converted gas was supplied to our system for determining the concentrations of CO, CO_2, CH_4, and H_2 (a Crystallux-4000M chromatograph equipped with a thermal conductivity detector). The conditions of analysis were Ar (special purity grade), a 150 × 0.4 cm packed column with SKT adsorbent, a temperature of 130°C, and a flow rate of 30 mL/min. The experimental error in determination of the gas product did not exceed ±5%. The temperature in the reactor and the heating unit was measured using chromel–alumel thermocouples, placed inside the reactor and controlled according to readings from thermocouples located on the outer wall of the reactor. Catalyst activity was determined as the ratio of the apparent degree of conversion of methane to the equilibrium value for this reaction.

It should be noted that after the tests, all of the catalysts were removed under anaerobic conditions (in an Ar inert gas stream) in order to prevent the formation of oxide species of the active components of the catalysts.

The aim of this work was to test laboratory sets of catalysts, compare them, and select samples displaying the properties most needed for the purposes of the SRM process.

ANALYTICAL APPROACH

Elemental analysis

CHNS analysis was performed on a Flash-2000 instrument with a chromatographic attachment (a PROPA-Q-10 He thermal conductivity detector). A weighed portion of 1.1–1.5 g was combusted in a tin capsule at a temperature of 2000°C with the addition of 10 mL of O_2.

Determination of Sulfur-Containing Compounds in Gaseous Products

Our analysis of gaseous products to determine if there were sulfur-containing compounds in them was performed via gas–solid chromatography on a Crystallux-4000M chromatograph equipped with a Varian HP-PLOT/Q capillary column (length, 30 m; diameter, 0.32 mm; adsorbent (polystyrene–divinylbenzene) bed thickness, 20 μm; carrier gas, He; flow rate, 95 cm^3/min). This allowed determination of sulfur-containing compounds at concentrations ≥10 ppm.

Structural Analysis of Catalysts

At all stages (after preparation, after reduction in an H_2 stream, and after catalytic testing), the phase composition of the catalyst systems was studied via X-ray diffraction (XRD) analysis on a DRON-3M diffractometer operating in the automatic mode using filtered CuK_α radiation. Phases were identified using the PDF-2 powder diffraction database [13].

^{57}Fe Mössbauer spectra were recorded on a Wissel electrodynamic-type spectrometer (Germany) at a temperature of 300 K. The radiation source was ^{57}Co(Rh) with an activity of 1.1 GBq. Isomer shifts were measured from the center of the magnetic hyperfine structure of metallic iron. The Mössbauer spectra were processed using standard least-square programs (LOREN (Semenov Institute of Chemical Physics, Russian Academy of Sciences), NORMOS (Germany)) by assuming a Lorentzian line shape.

Microphotographs of a catalyst's surface were recorded by transmission electron microscopy (TEM) on a JEOL JEM 2100F/UHR instrument with a resolution of 0.1 nm. Prior to study, 0.1 g of the sample was placed in 30 mL of C_2H_5OH and sonicated for 300 s. A droplet of the resulting mixture was placed on a standard TEM grid coated with amorphous carbon, dried for 1 h, placed in a microscope, and studied.

RESULTS AND DISCUSSION

The synthesized catalyst systems displayed high activity in the steam reforming of pure methane (without hydrogen sulfide admixtures). The product concentrations reached near-equilibrium values and remained unchanged throughout our catalytic tests (8 h). The test results are shown in Table 3.

It is evident from Table 3 that catalyst 2 displayed the highest activity. It should be noted that this catalyst contained the highest amount of Fe (7.61 wt %), which can positively affect the formation of the Fe-containing core–shell structures that are actively involved in the hydrocarbon reforming process. Catalyst 2 was thus selected to study the effect of sulfur-containing compounds on catalyst activity in reforming.

Catalyst 2 was tested in the reforming of methane with an H_2S admixture at a pressure of 2.0 MPa, a temperature of 800°C, an $H_2O : CH_4$ ratio of 2 : 1, and FHSV of 6000 h^{-1} for 30 h. The feedstock was a calibration gas mixture containing 30 ppm H_2S (OOO Monitoring). A state-of-the-art NIAP 03-01 catalyst used in Russian industry for the steam reforming of hydrocarbons was used for comparison. Figure 2 shows changes in methane conversion during a 30 h test.

Figure 2 shows commercial NIAP 03-01 catalyst was gradually poisoned with hydrogen sulfide, as evidenced by the drop in the degree of conversion of methane after 10 h on stream, while the activity of cat-

Table 3. Results from catalytic tests in the steam reforming of pure methane*

Catalyst number	T, °C	Dry gas composition, vol %				X	X/X_{eq}
		H_2	CO	CO_2	CH_4		
1	800	67.5	13.9	6.6	12.0	0.63	0.92
2	800	67.1	14.1	6.8	12.0	0.64	0.94
3	800	66.4	14.4	6.3	12.9	0.62	0.91
4	800	66.7	14.9	6.3	12.1	0.62	0.91
5	800	66.0	14.8	6.4	12.8	0.63	0.92
6	800	66.3	14.5	6.6	12.6	0.63	0.92

*X and X_{eq} are the apparent and equilibrium degrees of conversion, respectively.

alyst 2 remained stable throughout the test. This suggests the sample was resistant to poisoning with hydrogen sulfide impurities.

It should be noted that commercial NIAP 03-01 catalyst was tested earlier under similar conditions except for the presence of hydrogen sulfide ($CH_4 : H_2O = 1 : 2$; T = 800°C; FHSV = 6000 h^{-1}) [14]. The catalyst's activity did not change during prolonged tests (100 h). This suggests the drop in the activity of NIAP 03-01 catalyst can be attributed to the gradual poisoning of the active sites of the catalyst with hydrogen sulfide, rather than to coking.

Neither H_2S (from a Drechsel bottle with 10% $Cd(CH_3COO)_2$) nor SO_2 (from a Drechsel bottle with 10% $BaCl_2$) was detected in the converted gas at the outlet of the system. We therefore assumed that hydrogen sulfide was converted either to sulfur or to intermediates of the reaction with the converted gas components. CH_4 and CO_2 can thus react with hydrogen sulfide to form CS_2, while CO can be converted to COS. However, analysis of the converted gas via gas–solid chromatography revealed no CS_2 and COS impurities in the gas. We may therefore assume the selective conversion of hydrogen sulfide to elemental sulfur occurs during the process. This assumption is consistent with the data of [15, 16], which show the decomposition of hydrogen sulfide in the presence of catalysts containing iron oxides at temperatures above 400°C is characterized by a hydrogen sulfide conversion of >95% at an elemental sulfur selectivity of 95–99%. At these temperatures, the resulting sulfur is not deposited on the catalyst surface; instead, it is removed from the reaction zone in the gaseous form.

According to elemental analysis, the elemental sulfur content in the catalyst was 2.7 mg, or 0.017% of the total amount of sulfur passed through the reaction unit during the test. The presence of a trace amount of sulfur in the spent catalyst is apparently attributed to sulfur condensation upon reactor shutdown. This effect was observed in [17].

The absence of SO_2 in the converted gas suggests the hydrogen sulfide conversion process is characterized by high selectivity toward sulfur rather than sulfur dioxide, which can form in the subsequent oxidation of the resulting sulfur under the severe conditions of a moist reaction medium.

Most of the elemental sulfur formed because of hydrogen sulfide decomposition during SRM was isolated from the reaction unit of the system in the form of H_2S by exposing the unit to hydrogen in the absence of a catalyst at high pressure (2.0 MPa) and a temperature of 500°C. The hydrogen sulfide concentration in the effluent gas was determined iodometrically according to State Standard GOST 22387.2-97.

These results allow us to conclude preliminarily that the properties of catalyst 2 are similar those of catalyst synthesized from vermiculite ore. To confirm this hypothesis and study the evolution of the catalyst structure, the catalyst system was studied via XRD, Mössbauer spectroscopy, and TEM after all stages of preparation.

XRD analysis of the catalyst after its preparation (Fig. 3) showed that following the deposition of Ni on the substrate and stepwise calcination, the NiO phase (d = 2.41, 2.07, 1.47, 1.25) can clearly be seen in the

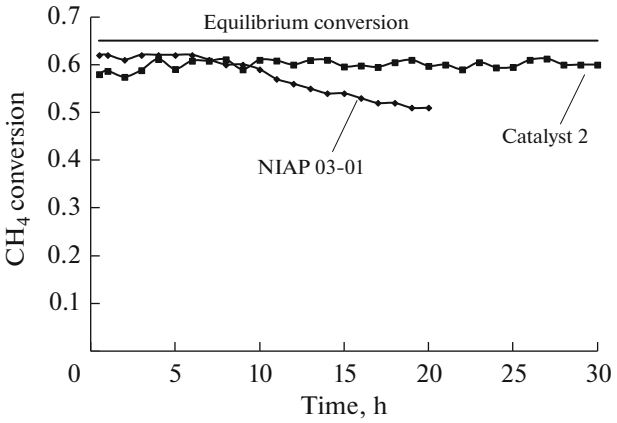

Fig. 2. Methane conversion versus time during the SRM process over catalyst 2 and NIAP 03-01 at an H_2S content in the mixture of 30 ppm.

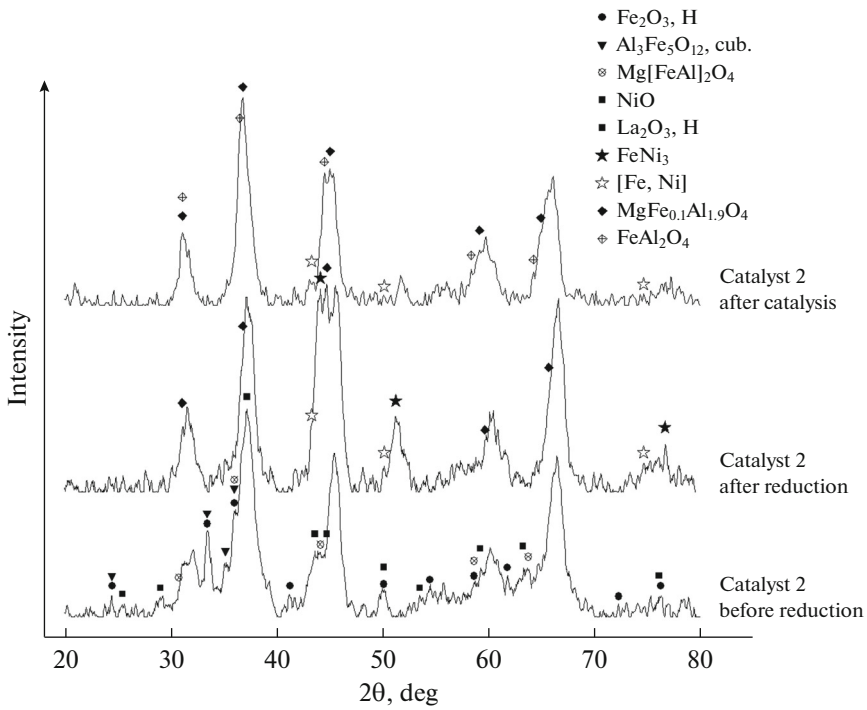

Fig. 3. Diffraction patterns of catalyst 2 before reduction, after reduction in a hydrogen environment at 800°C, and after SRM with an admixture of H_2S.

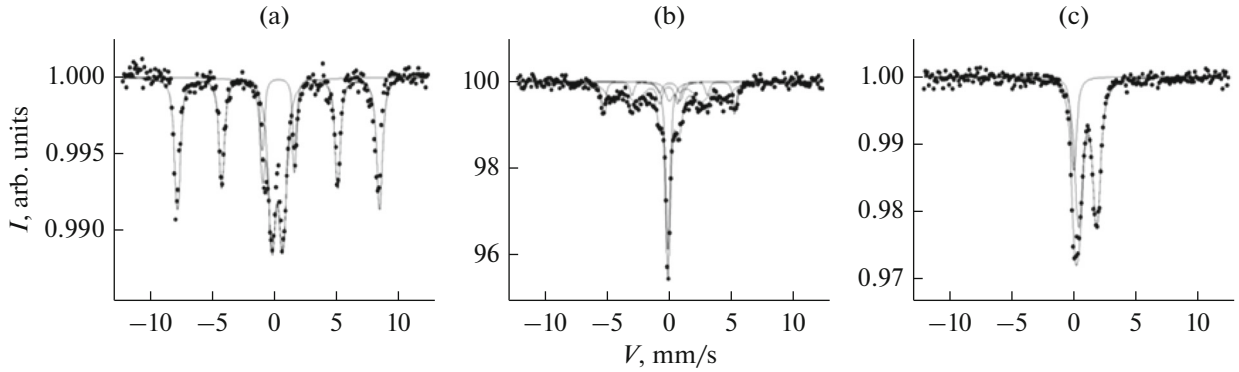

Fig. 4. Mössbauer spectra of catalyst 2 at $T = 300$ K: (a) before reduction, (b) after reduction in an H_2 environment, and (c) after testing in SRM with an admixture of H_2S.

sample's structure. In addition, oxide of the mixed $Mg[Fe,Al]_2O_4$ structure (d = 2.90, 2.48, 2.05, 1.57, 1.46) and iron oxide α-Fe_2O_3 (d = 3.63 , 2.67, 2.48, 2.18, 1.81, 1.68, 1.57, 1.50, 1.30, 1.24) were clearly identified [13]. Mössbauer spectroscopy revealed the paramagnetic Fe^{3+} ions that are part of the $Mg[Fe,Al]_2O_4$ spinel structure were in the sample before reduction (Fig. 4a; Table 4, sample a). The rest of the iron ions can be attributed to the magnetic structure of α-Fe_2O_3. The greatest changes in the structure of the sample occurred after 3 h of reduction in an H_2 environment at a temperature of 800°C.

According to XRD, NiO transitioned into metallic nickel, but the parameters were shifted. This could indicate partial replacement of the Ni atoms by Fe atoms, resulting in the formation of Fe–Ni alloys with different amounts of nickel. The composition of $Mg[Fe,Al]_2O_4$ magnesium–iron–aluminum spinel also changes by transitioning into $MgFe_{0.1}Al_{1.9}O_4$ spinel.

Like the XRD data, the Mössbauer spectroscopy data suggest the structure of the sample changed considerably. The Fe–Ni alloy with a face-centered cubic (fcc) lattice undergoes microseparation into a paramagnetic γ-Fe-Ni phase that corresponds to an alloy containing 10–15 at % Ni, and a magnetic γ-FeNi

Table 4. Mössbauer parameters of Fe species in catalyst 2 before reduction, after reduction in an H_2 environment at a temperature of 800°C, and after testing in the SRM process*

Sample	Fe species	δ	Δ	H_{in}, ±0.5 T	A, ±0.05
		±0.03 mm/s			
a	Fe^{3+}(paramagnetic)	0.31	0.93	–	0.43
	α-Fe_2O_3 (magnetic)	0.37	0.21	50.3	0.57
b	γ-FeNi (paramagnetic)	−0.06	–	–	0.27
	Fe^{3+}(paramagnetic)	0.39	0.87	–	0.10
	α-Fe (magnetic)	0.04	0.06	33.1	0.16
	γ-FeNi (magnetic)	−0.04	0.04	28.4	0.47
c	γ-FeNi (paramagnetic)	−0.09	−1.44	–	0.18
	Fe^{3+}(paramagnetic)	1.05		–	0.10

*Δ is the isomer shift with respect to α-Fe; Δ is the quadrupole splitting or quadrupole shift; H_{in} is the internal magnetic field at the ^{57}Fe nucleus; A is the relative content.

phase that corresponds to an alloy containing ≈70 at % Ni. The paramagnetic doublet of Fe^{3+} corresponds to γ-Fe_2O_3 nanoclusters ≈3–4 nm in size; the presence of α-Fe (magnetic) suggests the structure of the sample contains metallic iron.

XRD showed that after SRM with an admixture of hydrogen sulfide, catalyst sample 2 was characterized by the preservation of the $MgFe_{0.1}Al_{1.9}O_4$ spinel phase (d = 2.87, 2.43, 2.01, 1.56, 1.43) and the presence of metallic nickel (d = 2.03, 1.76, 1.24) and γ-FeNi (d = 2.08, 1.81, 1.27). In addition, the $FeAl_2O_4$ iron–aluminum spinel (d = 2.87, 2.45, 2.04, 1.58, 1.44) formed in the structure of the sample during the test.

Mössbauer spectroscopy indicated that after steam reforming, ≈18% of the sample consisted of particles of low-nickel γ-FeNi (paramagnetic) alloy containing 10–15 at % Ni, while ≈82% of it was nearly stoichiometric $FeAl_2O_4$ hercynite (Fig. 4, Table 4). This conclusion was based on the quadrupole splitting of the Fe^{2+} ion (Δ = 1.44 mm/s) being characteristic of the tetrahedral coordination of the iron complex in the structure of normal $FeAl_2O_4$ spinel [18]. It is important that no sulfur-containing compounds were found in the sample taken after the catalytic test. This confirmed the resistance of the catalyst to sulfur poisoning during the reforming of methane with an admixture of hydrogen sulfide.

To gain more detailed insight into the catalyst's structure after catalytic testing, the catalyst was studied via TEM and electron diffraction from particle surfaces (FFT).

According to electron diffraction data (Fig. 5), the external structure of a particle's surface corresponds to an fcc lattice. Calculations of the interplanar distances according to the FFT-image yield values of 1.8 and 2.1 Å, which are fairly close to the interplanar distances of the Ni(111) and Ni(200) faces characteristic of metallic nickel and nickel–iron alloys.

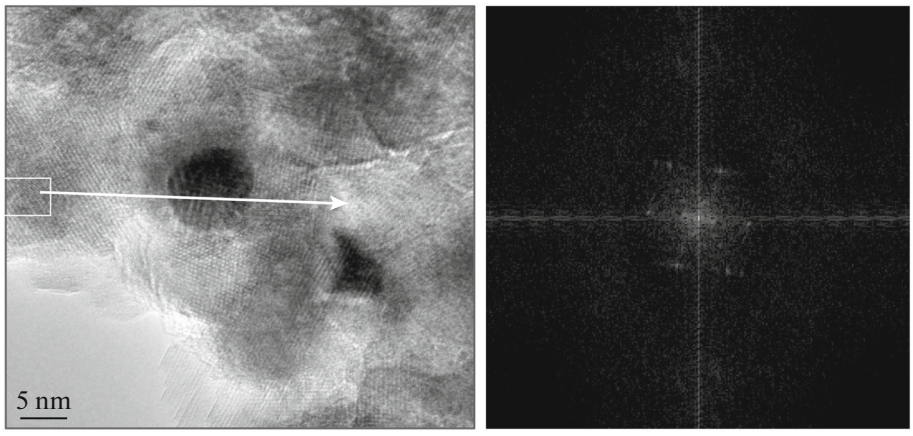

Fig. 5. Microphotograph of an individual particle in catalyst 2 and an FFT image of electron diffraction from a particle's surface.

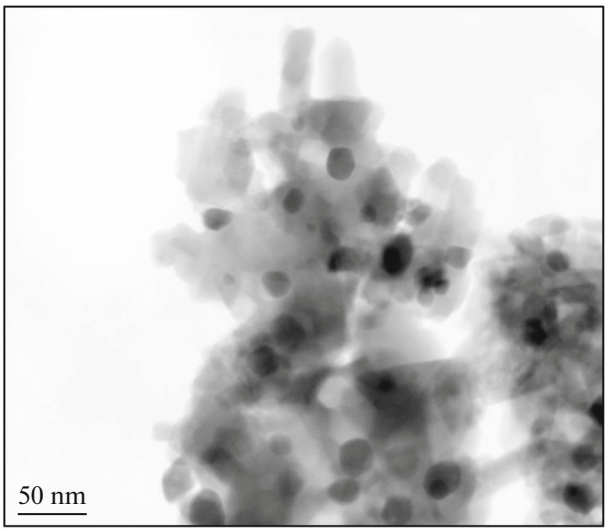

Fig. 6. Microphotograph of catalyst 2 after catalytic testing.

According to TEM (Fig. 6), the spatial arrangement of the Al, O, Fe, and Mg elements on a sample's surface remains the same after catalytic tests. No accumulations of individual phases containing Mg and Fe were observed. This suggests a homogeneous phase containing Al, O, Fe, and Mg is mostly formed, indicating the presence of $MgFe_xAl_{2-x}O_4$ spinel in the sample's structure and is consistent with the XRD and Mössbauer spectroscopy data. The nickel-containing phase is distributed over the surface in the form of small rounded particles, which can be attributed to the Ni and Fe alloys that form on the catalyst's surface.

CONCLUSIONS

Physicochemical explanations were developed for the formation of a highly efficient nickel-containing catalyst for the steam reforming of hydrocarbon feedstocks by the layer-by-layer deposition of components onto commercial spherical γ-Al_2O_3.

The resistance of the Ni–La catalyst to the presence of hydrogen sulfide was studied in a prolonged test (30 h) in the SRM process at a pressure of 2.0 MPa, a temperature of 800°C, an H_2O : CH_4 ratio of 2 : 1, FHSV of 6000 h^{-1}, and an H_2S concentration in the mixture of 30 ppm. It was shown that Ni–La catalyst is resistant to the presence of hydrogen sulfide in a steam–gas mixture, since the catalyst activity remains stable throughout the entire test.

The evolution of the catalyst during catalyst preparation, preactivation, and catalysis was studied. It was shown that the formation of Fe–Ni alloy particles tightly bound to the structure of the support on the catalyst surface was responsible for the polyfunctional properties of the catalyst, which displays high activity in both the SRM process and the oxidative decomposition of hydrogen sulfide to elemental sulfur.

REFERENCES

1. Zhang, Q.H., Li, Y., and Xu, B.Q., *Prepr. Pap.—Am. Chem. Soc., Div. Fuel Chem.,* 2004, vol. 49, no. 1, pp. 138–139.
2. Horn, R., Williams, K.A., Degenstein, N.J., and Schmidt, L.D., *J. Catal.,* 2006, vol. 242, no. 1, pp. 92–102.
3. Ishihara, A., Qian, E.W., Finahari, I.N., Sutrisna, I. P., and Kabe, T., *Fuel,* 2005, vol. 84, nos. 12–13, pp. 1462–1468.
4. Souza, M.M.V.M., Neto, O.R.M., and Schmal, M., *J. Nat. Gas Chem.,* 2006, vol. 15, no. 1, pp. 21–27.
5. Zeppieri, M., Villa, P.L., Verdone, N., Scarsella, M., and De Filippis, P., *Appl. Catal., A*, 2010, vol. 387, nos. 1–2, pp. 147–154.
6. Oliveira, E.L.G., Grande, C.A., and Rodrigues, A.E., *Can. J. Chem. Eng.,* 2009, vol. 87, no. 6, pp. 945–956.
7. Gangadharan, P., Kanchi, K.C., and Lou, H.H., *Chem. Eng. Res. Des.,* 2012, vol. 90, no. 11, pp. 1956–1968.
8. Tsodikov, M.V., Kurdyumov, S.S., Konstantinov, G.I., Murzin, V.Yu., Maksimov, Yu.V., Korchak, V.N., and Suzdalev, I.P., *Nanotechnol. Russ.,* 2012, vol. 7, nos. 9–10, pp. 463–470.
9. Shi, Q., Peng, Z., Chen, W., and Zhang, N., *J. Rare Earths,* 2011, vol. 29, no. 9, pp. 861–865.
10. Pino, L., Vita, A., Cipitì, F., Laganà, M., and Recupero, V., *Appl. Catal., B,* 2011, vol. 104, nos. 1–2, pp. 64–73.
11. Tsodikov, M.V., Kurdyumov, S.S., Murzin, V.Yu., Maksimov, Yu.V., Imshennik, V.K., Novichikhin, S.V., Maksimovskii, E.A., and Kriventsov, V.V., *Nanotechnol. Russ.,* 2012, vol. 7, nos. 9–10, pp. 471–481.
12. Pakhomov, N.A., *Nauchnye osnovy prigotovleniya katalizatorov: vvedenie v teoriyu i praktiku* (Scientific Foundations of Catalyst Preparation: Introduction to Theory and Practice), Novosibirsk: Sib, Otd. Ross. Akad. Nauk, 2011.
13. PDF-2 Data Base (Sets 1-47), International Centre for Diffraction Data, 1997.
14. Technology for the Preparation of New-Generation Nanostructured Natural Gas Conversion Catalysts. Report on State Contract no. 8411.1003702.16.240 (code "Conversion"), 2008.
15. Grunval'd, V.R., *Tekhnologiya gazovoi sery* (Gaseous Sulfur Technology), Moscow: Khimiya, 1992.
16. *Neftepererabotka i Neftekhimiya: Sbornik nauchnykh trudov* (Oil Refining and Petrochemistry: Collection of Research Papers), Khairudinov, I.R., Akhmetov, M.M., and Zaitseva, S.A., Eds., Ufa: Sterkh, 2001, vol. 33.
17. Amirov, Ya.S., Gimaev, R.N. and Saifullin, N.R., *Tekhniko-ekonomicheskie aspekty promyshlennoi ekologii* (Technical and Economic Aspects of Industrial Ecology), Ufa: Ufim. Gos. Neft. Tekhn. Univ., 1999, part 5.
18. Jastrzębska, I., Szczerba, J., Stoch, P., Błachowski, A., Ruebenbauer, K., Prorok, R., and Śnieżek, E., *Nukleonika,* 2015, vol. 60, no. 1, pp. 47–49.

Translated by M. Timoshinina